Theor Chem Acc (2009) 124:59–70
DOI 10.1007/s00214-009-0581-5

REGULAR ARTICLE

Hydrogen abstraction from $CF_3CF_2CFH_2$ and CF_3CFHCF_2H by OH radicals and Cl atoms: theoretical enthalpies and rate constants

Hong Gao · Ying Wang · Qin Wang · Jing-Yao Liu · Chia-Chung Sun

Received: 13 February 2009 / Accepted: 6 May 2009 / Published online: 31 May 2009

Abstract The hydrogen abstraction reactions of $CF_3CF_2CFH_2$ and CF_3CFHCF_2H with OH radicals and Cl atoms have been studied theoretically by a dual-level direct dynamics method. Two stable conformers of $CF_3CF_2CFH_2$ with C_s and C_1 symmetries and all possible abstraction channels for each reaction are all taken into consideration. Optimized geometries and frequencies of all the stationary points and extra points along minimum-energy path (MEP) have been computed at the BB1K/6-31+G(d, p) level of theory. To refine the energy profile of each reaction channel, single point energy calculations have been performed by the BMC-CCSD method. The rate constants are evaluated by canonical variational transition state theory (CVT) with the small-curvature tunneling correction method (SCT) over a wide temperature range of 200–1,000 K. The detailed branching ratios of four reactions are discussed. The good agreement found between our theoretical rate constants and the available experimental data suggests that the present approach could provide a reliable prediction for the $CF_3CFHCF_2H + Cl$ reaction about which there is little experimental information. The kinetic calculations show that the SCT effect plays an important role in all channels. In addition, in order to further reveal the thermodynamic properties, the enthalpies of formation of the reactants ($CF_3CF_2CFH_2$ and CF_3CFHCF_2H) and the product radicals (CF_3CF_2CFH, CF_3CFCF_2H, and CF_3CFHCF_2) are evaluated by applying isodesmic reactions at both BMC-CCSD//BB1K/6-31+G(d, p) and MC-QCISD//BB1K/6-31+G(d, p) levels of theory.

Keywords Direct dynamics · Rate constant · Variational transition-state theory · Hydrogen abstraction

1 Introduction

It is well known that chlorofluorocarbons (CFCs) are major contributors to the active chlorine budget in the stratosphere, and hence the release of them is a major cause of stratospheric ozone depletion, particularly in polar regions. Public concern over this issue has prompted industries to look for alternatives of CFCs in various applications. Partially fluorinated hydrocarbons (HFCs) are among the leading environmentally acceptable CFC alternatives from the point of view of ozone depletion. These compounds are superior to CFCs because they contain hydrogen atoms and can thus be removed by attacks by the radicals in the troposphere. However, their infrared absorbing properties raise concerns over such compounds as potential "greenhouse gases". Hence, their residence time in the atmosphere is a critical element in the assessment of their roles in radiative forcing and in the calculation of their global warming potentials (GWPs). The atmospheric lifetimes of the HFCs will be mainly controlled by the rates of the reactions with tropospheric species such as OH radical and Cl atom. These two reactions will, in general, be much faster than other degradation processes, such as ultraviolet photolysis or dissolution in the oceans or clouds. In this paper, we have conducted theoretically on the kinetics of the reactions of OH and Cl with $CF_3CF_2CFH_2$ (HFC-236cb) and CF_3CFHCF_2H (HFC-236ea). There was only one

Electronic supplementary material The online version of this article (doi:10.1007/s00214-009-0581-5) contains supplementary material, which is available to authorized users.

H. Gao · Y. Wang · Q. Wang · J.-Y. Liu (✉) · C.-C. Sun
State Key Laboratory of Theoretical and Computational Chemistry, Institute of Theoretical Chemistry, Jilin University, 130023 Changchun, People's Republic of China
e-mail: ljy121@jlu.edu.cn; ljy121@mail.jlu.edu.cn

experimental measurement for reaction OH + $CF_3CF_2CFH_2$ (R1). Garland et al. [1] carried out a rate study over the temperature range 251–314 K using laser photolysis laser-induced fluorescence techniques and proposed the Arrhenius expression of $k = (2.61 \pm 1.61) \times 10^{-13}$ exp [–(2.21 ± 0.40 kcal mol^{-1})/RT] cm^3 $molecule^{-1}$ s^{-1}, with a value of $k(300\ K) = 6.45 \times 10^{-15}$ cm^3 $molecule^{-1}$ s^{-1}. Based on their data, two evaluations are presented; the recommended rate constants at 298 K are 6.50×10^{-15} cm^3 $molecule^{-1}$ s^{-1} [2] and 4.40×10^{-15} cm^3 $molecule^{-1}$ s^{-1} [3], respectively. The fitting rate constant formula was given as $k = 1.30 \times 10^{-12}$ exp[–(3.38 kcal mol^{-1})/RT] cm^3 $molecule^{-1}$ s^{-1} in 200–300 K [3]. It is seen that the preexponential factor and activation energy reported in Ref. [1] is slightly lower than those estimated by Sander et al. [3]. With respect to CF_3CFHCF_2H + OH (R2), there were four experimental values available at room temperature. The rate constants (in cm^3 $molecule^{-1}$ s^{-1}) reported by Nelson et al. [4] [(5.30 ± 0.68) × 10^{-15}] and Hsu et al. [5] (5.10×10^{-15}) show mutual consistency, while they are somewhat lower than the results determined by Garland et al. [1] (6.80×10^{-15}) and Zhang et al. [6] (8.50×10^{-15}). Notice that, the recommended values, 5.00×10^{-15} [2] and 5.20×10^{-15} cm^3 $molecule^{-1}$ s^{-1} [3], are derived from the two formers data [4, 5]. Only one experimental rate constant was determined to be $(1.50 \pm 0.30) \times 10^{-15}$ cm^3 $molecule^{-1}$ s^{-1} [7] at 298 K for the reaction of $CF_3CF_2CFH_2$ with Cl (R3). In the case of the reaction CF_3CFHCF_2H + Cl (R4), however, no experimental study has been performed up to now. In view of the discrepancies of the available experimental results for R1–R3 as well as the lack of the kinetic study for R4, it is very desirable to perform deeper theoretical investigations for the title reactions so as to provide further kinetic information concerning them. To the best of our knowledge, no theoretical work has addressed above reactions.

For reactant $CF_3CF_2CFH_2$, two stable conformers are located, denoted as SC1 with C_s symmetry and SC2 with C_1 symmetry (see Fig. S1). Based on our electronic structure calculation, SC2 is only 0.11 kcal mol^{-1} stabler than SC1 at the BMC-CCSD//BB1K/6-31+G(d, p) level of theory, so both of them will contribute to the whole reaction. For SC1 with C_s symmetry, the two hydrogen atoms in the $–CFH_2$ position are equivalent, and as a result only one channel is identified for reaction SC1 + OH, that is,

$$CF_3CF_2CFH_2(C_s) + OH \rightarrow CF_3CF_2CFH + H_2O \quad (R1')$$

While in the case of conformer SC2, the two hydrogen atoms are not equivalent: one is located between the two F atoms and the other is in front of them, so the following two distinct reaction channels are feasible,

$$CF_3CF_2CFHH'(C_1) + OH \rightarrow CF_3CF_2CFH + H_2O \quad (R1a'')$$

$$\rightarrow CF_3CF_2CFH' + H_2O \quad (R1b'')$$

And for the species CF_3CFHCF_2H, hydrogen can be abstracted from –CFH– and $–CF_2H$ groups, respectively, i.e.,

$$CF_3CFHCF_2H + OH \rightarrow CF_3CFCF_2H + H_2O \quad (R2a)$$

$$\rightarrow CF_3CFHCF_2 + H_2O \quad (R2b)$$

Similar reaction channels can be found for reactions R3 and R4,

$$CF_3CF_2CFH_2(C_s) + Cl \rightarrow CF_3CF_2CFH + HCl \quad (R3')$$

$$CF_3CF_2CFHH'(C_1) + Cl \rightarrow CF_3CF_2CFH + HCl \quad (R3a'')$$

$$\rightarrow CF_3CF_2CFH' + HCl \quad (R3b'')$$

$$CF_3CFHCF_2H + Cl \rightarrow CF_3CFCF_2H + HCl \quad (R4a)$$

$$\rightarrow CF_3CFHCF_2 + HCl \quad (R4b)$$

The aim of our present work is to study the reaction mechanism and to obtain the kinetic information, such as the temperature dependence of the rate constants and branching ratios over a wide temperature range, the activation energies, as well as the reaction enthalpies. Here, a dual-level (X//Y) direct dynamics method [8–10] proposed by Truhlar et al. is applied to predict the rate constants of the above reactions. The comparison between theoretical and experimental results is discussed. In addition, it is known that the knowledge of the enthalpy of formation ($\Delta H^o_{f,298}$) of the species is important in the thermodynamic properties as well as in the kinetics of atmospheric processes. Due to the lack of theoretical or experimental $\Delta H^o_{f,298}$ values, we evaluated their enthalpies of formation theoretically by using isodesmic reactions [11].

2 Calculation methods

The electronic structure calculations are carried out by the Gaussian 03 program [12]. The geometries and frequencies of all the stationary points including reactants, transition states (TSs), products, and complexes are optimized by using the BB1K method [13] (Becke88 [14]–Becke95 [15] one-parameter model for kinetics methods) with the 6-31+G(d, p) basis set. As pointed out by Truhlar et al. [13], BB1K method is proved to be an effective density function theory (DFT) method for thermochemical kinetics and can give good saddle point geometries and barrier heights. At the same level of theory, the minimum energy path (MEP) is obtained by intrinsic reaction coordinate (IRC) theory to

confirm that the TS really connects to reactants and products along the reaction path. The first and second energy derivatives at geometries along the MEP are obtained to calculate the curvature of the reaction path and to calculate the generalized vibrational frequencies along the reaction path. In order to obtain more reliable energetic, single-point energies for the stationary points and a few extra points along with the MEP are computed by the BMC-CCSD method [16] (a multi-coefficient correlation method based on coupled cluster theory with single and double excitations (CCSD) proposed by Lynch and Truhlar) using the BB1K geometries. The potential profile is further refined with interpolated single-point energy (ISPE) method [17], which uses higher-level single-point energies at the lower-level saddle point plus a few selected points along the lower-level reaction path.

The initial information on the potential energy surface is used to evaluate the rate constants by means of the POLYRATE 9.3 program [18]. The theoretical rate constants are calculated by using canonical variational transition state theory (CVT) [19–21], which is the specific level of the variational transition state theory (VTST) [22–24]. The transmission coefficient is calculated by the centrifugal-dominant small curvature semiclassical adiabatic ground-state tunneling (SCT) [25, 26]. It should be noted that for a reaction which involves the transfer of a light particle between two heavy atoms, the large-curvature tunneling (LCT) [27, 28] probability might be important, especially at low temperature. While the LCT method requires more information of the potential energy surface (PES) and not just the MEP, beyond the scope of our work. Considering the fact that the SCT approach has been successfully used in the studies of many H-abstraction reactions [29–31], we chose SCT method in our present study. All the vibrational modes are treated as quantum-mechanical separable harmonic oscillators except for the two lowest vibrational ones. The hindered rotor approximation of Truhlar and Chuang [32, 33] is used for calculating the partition functions of these two modes. In the calculation of the electronic partition functions, the two electronic states for OH radical with a 140 cm^{-1} splitting in the $^2\Pi$ ground state are included, and the spin-orbit splitting of Cl, $^2P_{3/2}$ and $^2P_{1/2}$ with an 881 cm^{-1} splitting, is also considered.

In order to give theoretical predictions for the enthalpies of formation of reactants ($CF_3CF_2CFH_2$ (SC1 or SC2) and CF_3CFHCF_2H) and product radicals (CF_3CF_2CFH, CF_3CFCF_2H, and CF_3CHFCF_2), the high-level energies are calculated at both BMC-CCSD and MC-QCISD [34] (the multi-coefficient correlation method based on quadratic configuration interaction with single and double excitation) levels of theory based on BB1K/6-31+G(d, p) optimized geometries using the following isodesmic reactions:

$$CF_3CF_2CFH_2(\text{SC1 or SC2}) + CH_3CH_3 \rightarrow CF_3CF_3 + CH_3CH_2CH_3 \quad (R5)$$

$$CF_3CFHCF_2H + CH_3CH_3 \rightarrow CF_3CF_3 + CH_3CH_2CH_3 \quad (R6)$$

$$CF_3CF_2CFH + CH_3CH_3 \rightarrow CF_3CF_3 + CH_3CHCH_3 \quad (R7)$$

$$CF_3CFCF_2H + CH_3CH_3 \rightarrow CF_3CF_3 + CH_3CHCH_3 \quad (R8)$$

$$CF_3CHFCF_2 + CH_3CH_3 \rightarrow CF_3CF_3 + CH_3CHCH_3. \quad (R9)$$

3 Results and discussion

3.1 Stationary points

3.1.1 Geometries and vibrational frequencies

The calculated geometric parameters and harmonic vibrational frequencies of all reactants, translate-states, complexes, and products at the BB1K/6-31+G(d, p) level of theory are shown in Supporting Information (Fig. S1 and Table S1, respectively), as well as the available experimental values [35–38]. From Fig. S1 and Table S1, we can see that the agreement between the calculated and experimental geometries and frequencies data is good. And all the stationary points are identified as local minima (number of imaginary frequencies NIMAG = 0) and transition states (NIMAG = 1). The imaginary frequency can be seen as a measure of the thickness of barrier. A large imaginary frequency indicates a large negative force constant for the reaction coordinate mode and therefore a thin barrier [39]. As shown in Table S1, the transition state of each channel has a large imaginary frequency, which implies that the quantum tunneling effect should be important in the calculation of the rate constant.

For the structures of all the TSs, the following expected patterns are found:

3.1.1.1 $CF_3CF_2CFH_2/CF_3CFHCF_2H$ + OH reaction For the transition states abstracted by OH radical, it is found that the geometries of the TSs look more similar to those of reactants than to those of products. For TS1′, TS1a″, TS1b″, TS2a, and TS2b, the reactive C–H bond, which is broken, is elongated by 13, 12, 13, 14, and 13% compared to the C–H equilibrium bond length of the corresponding parent, and the forming bond H–O is longer than the equilibrium bond length of H_2O by 34, 34, 33, 31, and 33%, respectively, at the BB1K level of theory. The elongation of the breaking bond (C–H) is much less than the elongation of the forming bond

(H–O), indicating that these transition states are reactant-like, so these reactions may proceed via "early" transition states as expected for the exothermic reactions.

3.1.1.2 $CF_3CF_2CFH_2/CF_3CFHCF_2H + Cl$ reaction The transition states attacked by Cl atoms exhibit just opposite result, i.e., TS3′, TS3a″, TS3b″, TS4a, and TS4b are more similar to the product geometries than to reactant structures. The breaking C–H bonds are increased by 29, 29, 29, 30, and 29%, and the forming H–Cl bonds are stretched by 13, 13, 13, 12, and 13%, respectively, with respect to the corresponding regular bond length. Therefore, the transition states are product-like, and these reactions proceed via "late" transition states as expected for the endothermic reactions.

3.1.2 Enthalpies of formation

The reaction enthalpies (ΔH^o_{298}) for all channels at the BMC-CCSD//BB1K level of theory are listed in Table 1. We can see that the values of ΔH^o_{298} for reaction channels involved in H-abstraction from the rotation isomers SC1 and SC2 are very close; for example, the values of ΔH^o_{298} are −18.39, −18.74, and −18.50 kcal mol^{-1} for channels R1′, R1a″, and R1b″, respectively. Thus, in this work, we choose the lowest-energy product radical (in R1a″) as a representative to estimate its enthalpy of formation. It is known that isodesmic reaction, in which the number of each type of bond is conserved, will cancel the systematic errors in the ab initio calculations and lead to quite accurate results because of the similarity of bond type in both reactants and products. Therefore, we employ R5–R9 to estimate the $\Delta H^o_{f,298}$ values of the reactants and product radicals. First, we calculated reaction enthalpies of above reactions at the BMC-CCSD//BB1K level of theory, then these theoretical results are combined with the known standard enthalpies of formation [40] (CH_3CH_3, −20.04 ± 0.07 kcal mol^{-1}; CF_3CF_3, −321.35 kcal mol^{-1}; $CH_3CH_2CH_3$, −25.04 ± 0.12 kcal mol^{-1}; CH_3CHCH_3, 21.52 ± 0.48 kcal mol^{-1}) to estimate the $\Delta H^o_{f,298}$ values of these species. In order to further test the accuracy of the BMC-CCSD level of theory, MC-QCISD method is also applied to refine the energies based on the BB1K/6-31+G(d, p) geometries. The calculated results at two levels of theory are listed in Table 2. The calculated enthalpies of formation are −316.71, −317.34, −267.34, 265.03, and 265.81 kcal mol^{-1} for $CF_3CF_2CFH_2$, CF_3CFHCF_2H, CF_3CF_2CFH, CF_3CFCF_2H, and CF_3CHFCF_2, respectively, at the BMC-CCSD//BB1K level of theory, which are in good agreement with the results (−317.63, −318.25, −268.30, 265.94, and 266.53 kcal mol^{-1}) obtained at the MC-QCISD//BB1K level of theory; the largest deviation between them is within 1.0 kcal mol^{-1}. The good agreement between the results at two high-levels confirms the creditability of the enthalpies of formation obtained in the present study.

3.1.3 Potential energy surfaces

Schematic potential energy surfaces (PESs) of the title reactions with zero-point energy (ZPE) corrections are plotted in Fig. 1a–c. The energy of reactants is set to zero for reference. For all channels, the hydrogen-bonded complexes are located at the reactant or product side, which indicates each reaction will take place via an indirect

Table 2 Calculated enthalpies of formation at 298 K at BMC-CCSD//BB1K/6-31+G(d, p) and MC-QCISD//BB1K/6-31+G(d, p) levels of theory (in kcal mol^{-1})

Species	BMC-CCSD	MC-QCISD
$CF_3CF_2CFH_2$	−316.71	−317.63
CF_3CFHCF_2H	−317.34	−318.25
CF_3CF_2CFH	−267.34	−268.30
CF_3CFCF_2 H	−265.03	−265.94
CF_3CFHCF_2	−265.81	−266.53

Table 1 The enthalpies of reactions (ΔH^o_{298} in kcal mol^{-1}) calculated at the BMC-CCSD//BB1K/6-31+G(d, p) level of theory

Reactions	BMC-CCSD
$CF_3CF_2CFH_2$ (C_s) + OH → CF_3CF_2CFH + H_2O (R1′)	−18.39
CF_3CF_2CFHH' (C_1) + OH → CF_3CF_2CFH + H_2O (R1a″)	−18.74
CF_3CF_2CFH' + H_2O (R1b″)	−18.50
CF_3CFHCF_2H + OH → CF_3CFCF_2 H + H_2O (R2a)	−15.77
CF_3CFHCF_2 + H_2O (R2b)	−16.55
$CF_3CF_2CFH_2$ (C_s) + Cl → CF_3CF_2CFH + HCl (R3′)	−2.33
CF_3CF_2CFHH' (C_1) + Cl → CF_3CF_2CFH + HCl (R3a″)	−2.68
CF_3CF_2CFH' + HCl (R3b″)	−2.44
CF_3CFHCF_2H + Cl → CF_3CFCF_2 H + HCl (R4a)	0.30
CF_3CFHCF_2 + HCl (R4b)	−0.49

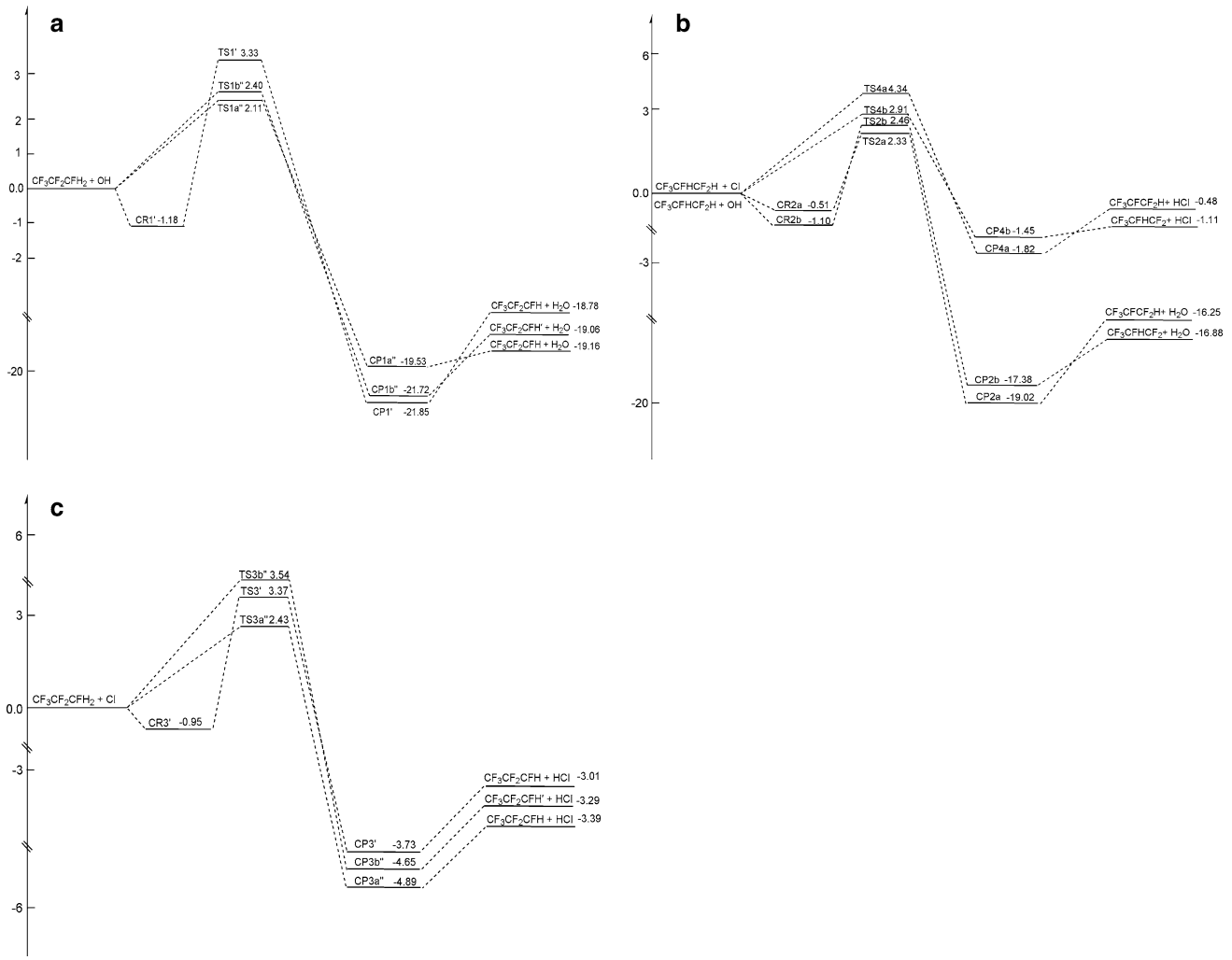

Fig. 1 Schematic pathways (**a**) for reactions $CF_3CF_2CFH_2$ (SC1 and SC2) + OH → products, (**b**) for reactions CF_3CFHCF_2H + OH/Cl → products, and (**c**) for reactions $CF_3CF_2CFH_2$ (SC1 and SC2) + Cl → products. Relative energies with ZPE correction at the BMC-CCSD//BB1K/6-311+G(d, p) level of theory are in kcal mol^{-1}

reaction mechanism. The barrier heights and exothermic values of the reaction channels will be discussed in the following two parts:

3.1.3.1 $CF_3CF_2CFH_2/CF_3CFHCF_2H$ + OH reaction For reaction $CF_3CF_2CFH_2$ (SC1 and SC2) + OH (R1), from Fig. 1a, it is seen that the barrier height of channel R1a″ (2.11 kcal mol^{-1}) is lower than those of R1b″ and R1′ by about 0.29 and 1.22 kcal mol^{-1}, and the former is more exothermic than the two latters by about 0.10 and 0.38 kcal mol^{-1}, respectively. Thus channel R1a″ is the most competitive both kinetically and thermodynamically. In addition, two channels R1a″ and R1b″ of SC2 have lower barrier heights and more exothermic values than R1′ of SC1, thus we infer that SC2 will have dominant contribution to the whole reaction of $CF_3CF_2CFH_2$ with OH radical. For two channels R2a and R2b, Fig. 1b shows that R2a has a lower barrier height (2.33 vs. 2.46 kcal mol^{-1}), while R2b has larger exothermicity (−16.25 vs. −16.88 kcal mol^{-1}). Thus, we predict that these two channels may be competitive.

3.1.3.2 $CF_3CF_2CFH_2/CF_3CFHCF_2H$ + Cl reaction For reaction $CF_3CF_2CFH_2$ (SC1 and SC2) + Cl (R3) (see Fig. 1c), these three channels take the barrier heights of 3.37, 2.43, and 3.54 kcal mol^{-1} for R3′, R3a″ and R3b″, respectively, while the exothermic values of them are almost the same; thus, R3a″ will be the dominant channel for R3. On other hand, the barrier height of channel R3′ of SC1 is between those of R3a″ and R3b″of SC2, thus, it is expected that the contribution of SC1 and SC2 to the total rate constants may be competitive. For reaction

CF_3CFHCF_2H + Cl (R4) (see Fig. 1b), by similar comparison for the barrier heights and exoergic values, R4b is expected to be predominant channel.

Furthermore, it is found that R3 and R4 possess higher potential barriers and less quantity of heat than those of R1 and R2, indicating that the reactions of these two HFCs with Cl atoms are more difficultly to occur than the reactions of them with OH radicals.

3.2 Rate constants calculation

The PES information for R1–R4 obtained at the BMC-CCSD//BB1K/6-31+G(d,p) level of theory is put into the POLYRATE 9.3 program to perform the dynamic calculation over a wide temperature range from 200 to 1,000 K. The theoretical rate constants for each reaction channel are evaluated by canonical variational transition state theory (CVT) with the small-curvature tunneling (SCT) correction. In the rate constant calculation, the symmetry factor (σ) is equal to 1 for the reactant (σ_R) and for the transition state (σ_{TS}). However, note that for conformer SC1 with C_s symmetry, the transition state has two chiral stereoisomers (i.e., $m_{TS} = 2$), thus, as explained by Miller [41] and Gilbert et al. [42], the total reaction path degeneracy (n), which is defined as $\frac{\sigma_R}{\sigma_{TS}} \cdot \frac{m_{TS}}{m_R}$, is equal to 2. In addition, the accuracy of the calculated rate constants was monitored by means of the mean unsigned percentage error (MUPE) [43], which is very familiar and used more extensively, defined as

$$\mathrm{MUPE} = \left(\frac{1}{N} \sum_{i=1}^{N} \left| \frac{k_i^{\mathrm{calc}} - k_i^{\mathrm{exp}}}{k_i^{\mathrm{exp}}} \right| \right) \times 100\% \qquad \text{(E1)}$$

where k_i^{calc} represents the calculated rate constant at a certain temperature, k_i^{exp} represents the experimental result at the same temperature, and N is the number of rate constants for which the comparison is made. For comparison, the calculated rate constants, available experimental values [1, 4–7] and MUPE are listed in Tables 3, 4, and 5.

3.2.1 $CF_3CF_2CFH_2/CF_3CFHCF_2H$ + OH reaction

3.2.1.1 Variational and tunneling correction Firstly, we presented a detailed analysis for channel R1′. Figure 2 depicts the classical potential energy curve [$V_{MEP}(s)$], the vibrationally adiabatic ground-state potential energy curve [$V_a^G(s)$], and the zero-point energy [ZPE(s)] curve for channel R1′ as a function of the intrinsic reaction coordinate s, where $V_a^G(s) = V_{MEP}(s) + \mathrm{ZPE}(s)$. It is seen that channel R1′ has a low barrier height and smooth potential energy profile in the reactant region. The maximum positions of the V_{MEP} and V_a^G curves have a little shift, which indicates that the variational effect would be important in the rate constant calculation for R1′. The similar plots can be drawn for the other channels (R1b″, R1a″, R2a, and R2b) and therefore are not shown in present paper.

Table 3 Calculated and experimental rate constants (in cm^3 $molecule^{-1}$ s^{-1}) as well as the average error for reaction $CF_3CF_2CFH_2$ (SC1 or SC2) + OH → products in the temperature range of 200–1,000 K at the BMC-CCSD//BB1K/6-311+G(d, p) level of theory

T(K)	k_1'	k_1''	k_{1T}	Exptl.
200	8.50×10^{-17}	5.83×10^{-16}	5.38×10^{-16}	
225	2.27×10^{-16}	1.15×10^{-15}	1.04×10^{-15}	
250	5.20×10^{-16}	2.13×10^{-15}	1.91×10^{-15}	
251	5.37×10^{-16}	2.19×10^{-15}	1.96×10^{-15}	3.13×10^{-15}[a]
260	7.00×10^{-16}	2.69×10^{-15}	2.40×10^{-15}	
270	9.26×10^{-16}	3.36×10^{-15}	2.99×10^{-15}	
275	1.06×10^{-15}	3.73×10^{-15}	3.31×10^{-15}	4.60×10^{-15}[a]
286	1.40×10^{-15}	4.67×10^{-15}	4.12×10^{-15}	
298	1.87×10^{-15}	5.88×10^{-15}	5.17×10^{-15}	
300	1.96×10^{-15}	6.11×10^{-15}	5.37×10^{-15}	6.45×10^{-15}[a]
314	2.66×10^{-15}	7.84×10^{-15}	6.87×10^{-15}	7.60×10^{-15}[a]
325	3.35×10^{-15}	9.43×10^{-15}	8.24×10^{-15}	
340	4.49×10^{-15}	1.20×10^{-14}	1.05×10^{-14}	
350	5.39×10^{-15}	1.40×10^{-14}	1.21×10^{-14}	
365	7.02×10^{-15}	1.74×10^{-14}	1.51×10^{-14}	
400	1.17×10^{-14}	2.75×10^{-14}	2.37×10^{-14}	
500	3.77×10^{-14}	7.86×10^{-14}	6.70×10^{-14}	
600	8.97×10^{-14}	1.75×10^{-13}	1.48×10^{-13}	
800	3.17×10^{-13}	5.74×10^{-13}	4.81×10^{-13}	
1,000	7.90×10^{-12}	1.39×10^{-12}	1.15×10^{-12}	
MUPE			23%	

[a] From Ref. [1]

Because reaction channels R1′ and R1b″ are the favorable channels and R1a″, R2a, and R2b have similar variational and tunneling effects to them, here, we chose these two reaction channels as representatives to in detail analyze. The TST, CVT, and CVT/SCT rate constants of channels R1′ and R1b″ are presented in Fig. 3a, b. For R1′ (see Fig. 3a), the variational effect deviates the CVT rate constant from the TST one by factors of 0.39 at 200 K, 0.78 at 400 K, and 0.98 at 1,000 K for R1′, respectively. These ratios indicate the variational effect is important at low temperatures and almost negligible at the high temperature range. Moreover, by contrasting the CVT and CVT/SCT, it is shown that the SCT correction must be taken into account in the rate constant calculations in the low temperature range, but as the temperature increases, the two curves are asymptotic to each other. For example, the ratios of $k_{CVT/SCT}/k_{CVT}$ are 6.17 at 200 K, 1.31 at 500 K, and 1.03 at 1,000 K for R1′, respectively. Similar conclusions can be drawn for R1a″ and R2a. For channel R1b″ (see Fig. 3b), the case is slightly different, both the variational effect and SCT effect play an important role

Table 4 Calculated and experimental rate constants (in cm^3 $molecule^{-1}$ s^{-1}) as well as the average error for reaction $CF_3CFHCF_2H + OH \rightarrow$ products in the temperature range of 200–1,000 K at the BMC-CCSD//BB1K/6-311+G(d, p) level of theory

T(K)	k_{2a}	k_{2b}	k_{2T}	Exptl.
200	1.63×10^{-16}	1.13×10^{-16}	2.76×10^{-16}	
225	3.88×10^{-16}	2.73×10^{-16}	6.61×10^{-16}	
250	7.98×10^{-16}	5.75×10^{-16}	1.37×10^{-15}	
251	8.20×10^{-16}	5.91×10^{-16}	1.41×10^{-15}	3.59×10^{-15}[a]
260	1.03×10^{-15}	7.51×10^{-16}	1.78×10^{-15}	$(5.04 \pm 0.76) \times 10^{-15}$[d]
270	1.31×10^{-15}	9.67×10^{-16}	2.28×10^{-15}	$(5.22 \pm 0.59) \times 10^{-15}$[d]
275	1.47×10^{-15}	1.09×10^{-15}	2.56×10^{-15}	5.10×10^{-15}[a]
283	1.75×10^{-15}	1.31×10^{-15}	3.06×10^{-15}	$(6.58 \pm 0.87) \times 10^{-15}$[d]
286	1.87×10^{-15}	1.41×10^{-15}	3.28×10^{-15}	6.06×10^{-15}[c]
298	2.39×10^{-15}	1.83×10^{-15}	4.22×10^{-15}	6.80×10^{-15}[a]
				$(5.30 \pm 0.68) \times 10^{-15}$[b]
				5.10×10^{-15}[c]
				$(8.51 \pm 0.26) \times 10^{-15}$[d]
300	2.49×10^{-15}	1.90×10^{-15}	4.39×10^{-15}	6.93×10^{-15}[a]
				7.94×10^{-15}[c]
305	2.74×10^{-15}	2.11×10^{-15}	4.85×10^{-15}	$(8.87 \pm 1.26) \times 10^{-15}$[d]
314	3.24×10^{-15}	2.52×10^{-15}	5.76×10^{-15}	8.06×10^{-15}[a]
325	3.93×10^{-15}	3.11×10^{-15}	7.04×10^{-15}	1.22×10^{-14}[c]
330	4.28×10^{-15}	3.41×10^{-15}	7.69×10^{-15}	$(1.39 \pm 0.36) \times 10^{-14}$[d]
340	5.04×10^{-15}	4.07×10^{-15}	9.11×10^{-15}	
350	5.89×10^{-15}	4.82×10^{-15}	1.07×10^{-14}	1.75×10^{-14}[c]
364	7.24×10^{-15}	6.04×10^{-15}	1.33×10^{-14}	2.10×10^{-14}[c]
365	7.35×10^{-15}	6.13×10^{-15}	1.35×10^{-14}	$(2.18 \pm 0.28) \times 10^{-14}$[d]
400	1.17×10^{-14}	1.02×10^{-14}	2.19×10^{-14}	
500	3.31×10^{-14}	3.30×10^{-14}	6.61×10^{-14}	
600	7.23×10^{-14}	8.05×10^{-14}	1.53×10^{-13}	
800	2.27×10^{-13}	3.02×10^{-13}	5.29×10^{-13}	
1,000	5.24×10^{-12}	7.91×10^{-13}	1.32×10^{-12}	
MUPE			44%	

[a] From Ref. [1]

[b] From Ref. [4]

[c] From Ref. [5]

[d] From Ref. [6]

over the whole temperature range. For example, the values of k_{CVT}/k_{TST} are 0.41 at 200 K and 0.83 at 1,000 K, and the $k_{CVT/SCT}/k_{CVT}$ ratios are 147.76 at 200 K and 1.45 at 1,000 K. Similarly, R2b also has the same property.

3.2.1.2 Total rate constants and branching ratios $CF_3CF_2CFH_2 + OH$ reaction In the case of $CF_3CF_2CFH_2$, the energy of SC1 is very close to that of SC2, so they will both contribute to the overall reaction rate constant. When $CF_3CF_2CFH_2$ is attacked by OH radicals or Cl atoms, the total rate constant can be obtained from the following expression,

$$\begin{aligned} k_{nT} &= \omega_1 k'_n + \omega_2 k''_n \\ &= \omega_1 k'_n + \omega_2 \left(k''_{na} + k''_{nb}\right) \\ &= k'_{nT} + k''_{nT} \quad (n = 1 \text{ or } 3) \end{aligned} \tag{E2}$$

where ω_1 and ω_2 are the weight factors of each conformer calculated from the Boltzmann distribution function. The calculated rate constants of each conformer and the total rate constants of R1 are presented in Table 3, along with the available experimental values [1] and the average error. It is found that the calculated rate constants in the temperature range of 251–314 K are in good agreement with the experimental data [1], with the MUPE of 23%. In 200–300 K, the

Table 5 Calculated and experimental rate constants (in cm^3 $molecule^{-1}$ s^{-1}) as well as the average error for reactions $CF_3CF_2CFH_2$ (SC1 or SC2) + Cl → products and CF_3CFHCF_2H + Cl → products in the temperature range of 200–1,000 K at the BMC-CCSD//BB1K/6-311+G(d, p) level of theory

T(K)	k_3'	k_3''	k_{3T}	Exptl.	k_{4a}	k_{4b}	k_{4T}
200	5.80×10^{-17}	1.29×10^{-16}	1.22×10^{-16}		5.22×10^{-18}	4.93×10^{-17}	5.45×10^{-17}
225	1.66×10^{-16}	2.98×10^{-16}	2.83×10^{-16}		2.04×10^{-17}	1.49×10^{-16}	1.69×10^{-16}
250	4.04×10^{-16}	6.02×10^{-16}	5.75×10^{-16}		6.26×10^{-17}	3.73×10^{-16}	4.36×10^{-16}
260	5.54×10^{-16}	7.77×10^{-16}	7.44×10^{-16}		9.30×10^{-17}	5.17×10^{-16}	6.10×10^{-16}
275	8.61×10^{-16}	1.11×10^{-15}	1.07×10^{-15}		1.61×10^{-16}	8.12×10^{-16}	9.73×10^{-16}
298	1.58×10^{-15}	1.80×10^{-15}	1.76×10^{-15}	$(1.50 \pm 0.30) \times 10^{-15}$ [a]	3.38×10^{-16}	1.51×10^{-15}	1.85×10^{-15}
314	2.30×10^{-15}	2.45×10^{-15}	2.42×10^{-15}		5.35×10^{-16}	2.21×10^{-15}	2.75×10^{-15}
325	2.94×10^{-15}	2.98×10^{-15}	2.97×10^{-15}		7.18×10^{-16}	2.83×10^{-15}	3.55×10^{-15}
340	4.01×10^{-15}	3.84×10^{-15}	3.87×10^{-15}		1.04×10^{-15}	3.87×10^{-15}	4.91×10^{-15}
350	4.88×10^{-15}	4.50×10^{-15}	4.58×10^{-15}		1.32×10^{-15}	4.71×10^{-15}	6.03×10^{-15}
365	6.43×10^{-15}	5.64×10^{-15}	5.81×10^{-15}		1.83×10^{-15}	6.21×10^{-15}	8.04×10^{-15}
400	1.15×10^{-14}	9.08×10^{-15}	9.66×10^{-15}		3.62×10^{-15}	1.11×10^{-14}	1.47×10^{-14}
500	4.22×10^{-14}	2.63×10^{-14}	3.08×10^{-14}		1.58×10^{-14}	3.92×10^{-14}	5.50×10^{-14}
600	1.09×10^{-13}	5.73×10^{-14}	7.37×10^{-14}		4.47×10^{-14}	9.62×10^{-14}	1.41×10^{-13}
800	4.16×10^{-13}	1.70×10^{-13}	2.59×10^{-13}		1.78×10^{-13}	3.24×10^{-13}	5.02×10^{-13}
1,000	1.05×10^{-12}	3.59×10^{-13}	6.26×10^{-13}		4.40×10^{-13}	7.25×10^{-13}	1.17×10^{-12}
MUPE			24%				

[a] From Ref. [7]

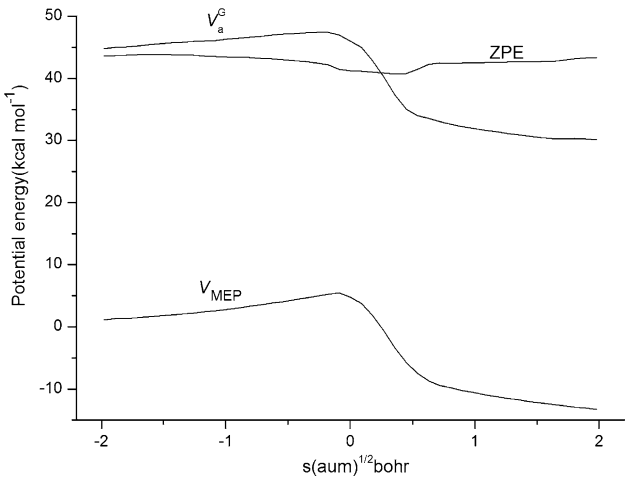

Fig. 2 Classical potential energy curve (V_{MEP}), ground-state vibrationally adiabatic energy curve (V_a^G), and zero-point energy curve (ZPE) as functions of s (amu)$^{1/2}$ bohr at the BMC-CCSD//BB1K/6-31+G(d, p) level of theory for reaction $CF_3CF_2CFH_2$ (C_s) + OH → products (R1′)

calculated activation energy (E_a) 2.74 kcal mol^{-1}, which is fitted by the CVT/SCT rate constants, is slightly lower than the value of 3.38 kcal mol^{-1} recommended by Sander et al. [3]. In 251–314 K, the theoretical E_a (3.12 kcal mol^{-1}) is slightly larger than experimental result (2.21 ± 0.40 kcal mol^{-1}) proposed by Garland et al. [1].

The temperature dependence of the branching ratios is plotted in Fig. S2a as Supporting Information for reaction $CF_3CF_2CFH_2$ (SC2) + OH (R1″). It is found that the ratios of k_{1a}''/k_1'' are 0.66 at 200 K and 0.55 at 1,000 K, respectively, indicating that channel R1a″ is major channel over the whole temperature range for R1″. From expression E2, it is easy to evaluate the degree of each conformer contributing to the total rate constant. For example, the ω_1 and ω_2 are 0.09 and 0.91 at 200 K, and 0.39 and 0.61 at 1,000 K, respectively. In addition, the contribution of each conformer to the total rate constants is depicted in Fig. 4a. The change of k_{1T}''/k_{1T} is from 0.99 to 0.74 within 200–1,000 K, which indicates that the hydrogen abstraction from conformer SC2 dominates the reaction over the whole temperature range.

CF_3CFHCF_2H + OH reaction For reaction CF_3CFHCF_2H + OH (see Table 4), the rate constant k(298 K) = 4.22×10^{-15} cm^3 $molecule^{-1}$ s^{-1} is very close to the experimental values of $(5.30 \pm 0.68) \times 10^{-15}$ and 5.10×10^{-15} cm^3 $molecule^{-1}$ s^{-1} reported by Nelson et al. [4] and Hsu et al. [5], respectively. The calculated MUPE is 44%. Furthermore, the calculated activation energies (E_a) along with three experimental values [1, 5, 6] and two recommended values [2, 3] are listed in Table 6. It is seen that our theoretical E_a values and four reference data [2, 3, 5, 6] show mutual agreement in the measured temperature ranges, while all of them are about 1.5 times larger than the result from Ref. [1].

The branching ratios for this reaction are plotted in Fig. 4b. We can see that R2a is the more important channel

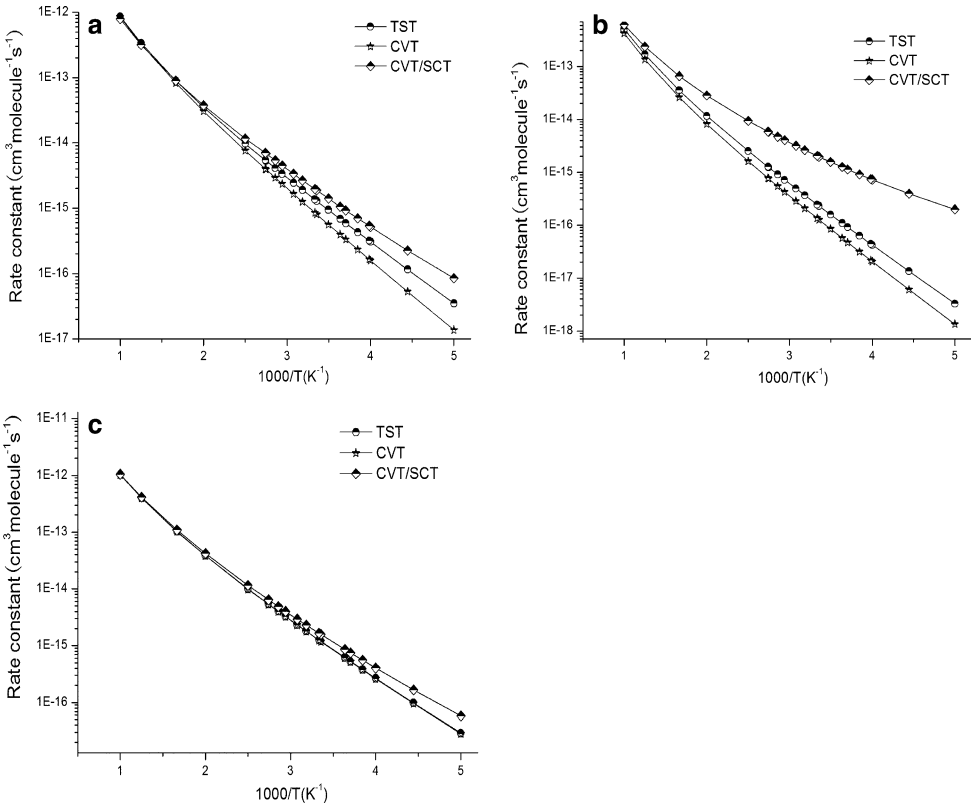

Fig. 3 Plots of TST, CVT and CVT/SCT rate constants calculated at the BMC-CCSD//BB1K/6-31+G(d, p) level of theory versus 1,000/T between 200 and 1,000 K (**a**) for reaction $CF_3CF_2CFH_2$ (C_s) + OH → products (R1′), (**b**) for reaction $CF_3CF_2CFH_2$ (C_1) + OH → products (R1b″), (**c**) for reaction $CF_3CF_2CFH_2$ (C_s) + Cl → products (R3′)

than R2b at the low temperature range. The values of k_{2a}/k_{2T} and k_{2b}/k_{2T} are 0.59 and 0.41 at 200 K. However, as the temperature increases, the ratio of k_{2b}/k_{2T} is larger than k_{2a}/k_{2T} and then R2b becomes a major reaction channel. For example, the values of k_{2a}/k_{2T} and k_{2b}/k_{2T} are 0.40 and 0.60 at 1,000 K, respectively.

3.2.2 $CF_3CF_2CFH_2$/CF3CFHCF$_2$H + Cl reaction

3.2.2.1 Variational and tunneling correction The plot of TST, CVT, and CVT/SCT rate constants for channel R3′ is shown in Fig. 3c. It shows that the rate constants of TST and CVT are nearly the same over the whole temperature range, which means that the variational effect is very small or almost negligible. This character can also be analysed from the $V_a^G(s)$, $V_{MEP}(s)$, and ZPE(s) curves. Different from R1′, the maximum positions of the $V_a^G(s)$ and $V_{MEP}(s)$ curves are almost the same, implying a small variational effect. The CVT/SCT rate constants are greater than the CVT rate constants in the low temperature range. For example, the ratios of $k_{CVT/SCT}/k_{CVT}$ are 2.06 at 200 and 1.16 at 400 K. Thus, SCT effect plays an important role for R3′ at the low temperature range. While for R3a″, R3b″, R4a, and R4b, both the variational effect and SCT effect play an important role over the whole temperature range.

3.2.2.2 Total rate constants and branching ratios As to the reactions of Cl atoms with $CF_3CF_2CFH_2$ and CF_3CFHCF_2H, the theoretical results and available experimental value [7] are listed in Table 5.

$CF_3CF_2CFH_2$ + Cl reaction Similar to reaction $CF_3CF_2CFH_2$ + OH, the total rate constants are obtained from E2. From Table 5, it is found that the calculated value 1.76×10^{-15} cm^3 molecule^{-1} s^{-1} agrees quite well with the only experimental datum [7] $(1.50 \pm 0.30) \times 10^{-15}$ cm^3 molecule^{-1} s^{-1} at 298 K. The MUPE is 24%. For reaction $CF_3CF_2CFH_2$ (SC2) + Cl (R3b″), Fig. S2b (in Supporting Information) shows the ratios of k_{3a}''/k_3'' are 0.93 at 200 K and 0.72 at 1,000 K, and thus R3a″ will be the dominant channel of R3″ over the whole temperature range. In addition, the contribution of conformers SC1 and SC2 to the total rate constant is exhibited in Fig. 4c. As can be seen that below 650 K, the contribution of SC2 to the overall reaction is important; for example, the values of k_{3T}''/k_{3T} are 0.96 at 200 K and 0.61 at 500 K, respectively. However, as the temperature increases, SC1 prevails over SC2 and then becomes the major one; the ratio of k_{3T}'/k_{3T} is 0.65 at 1,000 K. It is clear that the role of SC2 in the reaction $CF_3CF_2CFH_2$ + Cl is much less important than its role in the reaction $CF_3CF_2CFH_2$ + OH.

CF_3CFHCF_2H + Cl reaction For this reaction, there is no available experimental rate constant in the literature;

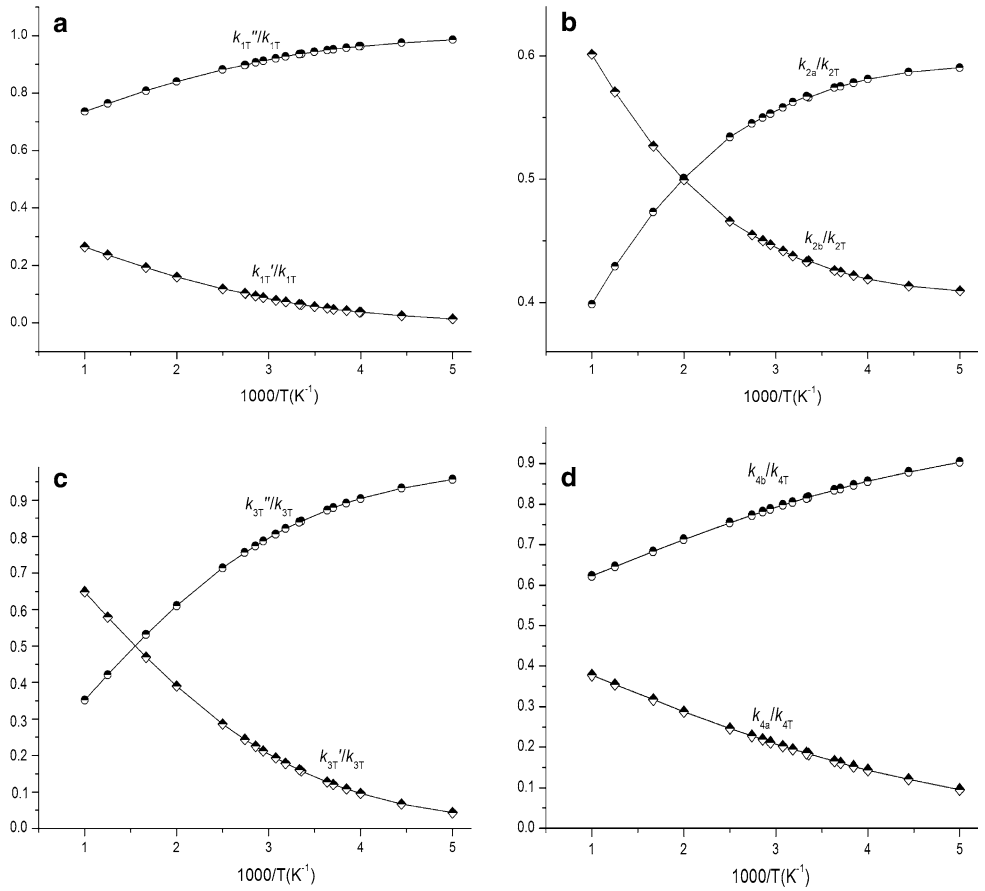

Fig. 4 Plots of the calculated branching ratios versus 1,000/T between 200 and 1,000 K (**a**) for reaction $CF_3CF_2CFH_2 + OH \rightarrow$ products, (**b**) for reaction $CF_3CFHCF_2H + OH \rightarrow$ products, (**c**) for reaction $CF_3CF_2CFH_2 + Cl \rightarrow$ products, and (**d**) for reaction $CF_3CFHCF_2H + Cl \rightarrow$ products

Table 6 The calculated activation energies (in kcal mol^{-1}) along with the reference data for reaction $CF_3CFHCF_2H + OH$

T (K)	E_a	Reference
251–314	3.50	This work
	2.01 ± 0.30	Garland et al. [1]
290–380	3.67	This work
	3.34	Atkinson et al. [2]
200–300	3.29	This work
	3.08	Sander et al. [3]
286–364	3.71	This work
	3.30	Hsu et al. [5]
260–365	3.34	This work
	2.84 ± 0.31	Zhang et al. [6]

consequently, no comparison with the calculated result is made. While owing to the good consistency between theoretical and experimental values for the other three reactions, one may expect that the present theoretical calculation can provide reliable prediction for the rate constant of this reaction. Figure 4d shows the temperature dependence of k_{4a}/k_{4T} and k_{4b}/k_{4T}. We find that the contribution of channel R4b to the overall reaction is important than R4a. The k_{4b}/k_{4T} ratios are 0.90 at 200 K and 0.62 at 1,000 K, indicating that R4b is a major channel over the whole temperature range.

From Tables 3, 4, and 5, we can also see that the reactions of $CF_3CF_2CFH_2/CF_3CFHCF_2H$ with OH radicals are easier to occur than $CF_3CF_2CFH_2/CF_3CFHCF_2H$ with Cl atoms. For example, the k_{1T} and k_{2T} are about 2.9 and 2.3 times than k_{3T} and k_{4T} at room temperature, respectively. In addition, in the direct dynamics calculation, errors may produce from electronic structure calculation of barrier height and tunneling corrections. The BMC-CCSD method is known to have mean unsigned error in calculating barrier height of 0.71 kcal mol^{-1} [16]; on other hand, the SCT method may also provide an inadequate account for the tunneling and be less accurate than the LCT method. However, these errors may compensate each other in the rate constant calculation [44]. In view of the largest MUPE less than 44%, the possibility of error cancellation appears acceptable and satisfied for the present study.

Since there is few data available at other temperature, for convenience of future experimental measurements, the three-parameter expressions for the CVT/SCT rate constants for the title reactions within 200–1,000 K are given as below (in cm^3 $molecule^{-1}$ s^{-1}):

$$k_{1T} = 4.08 \times 10^{-22} T^{3.24} \exp(-631/T)$$
$$k_{2T} = 6.46 \times 10^{-21} T^{2.90} \exp(-941/T)$$
$$k_{3T} = 5.53 \times 10^{-22} T^{3.15} \exp(-882/T)$$
$$k_{4T} = 3.30 \times 10^{-18} T^{2.10} \exp(-1669/T)$$

4 Conclusions

In this paper, dual-level direct dynamics method is employed in the study of the hydrogen abstraction reactions of $CF_3CF_2CFH_2/CF_3CFHCF_2H + X$ (X = OH and Cl). The present work can be summarized as follows:

(1) The electronic structure calculations are carried out at the BB1K/6-31+G(d, p) level of theory and higher level energies of the stationary points and the points selected on the MEP are calculated at the BMC-CCSD//BB1K level of theory. Then, the theoretical rate constants are calculated in the temperature range from 200 to 1,000 K by canonical variational transition state theory (CVT) with a small-curvature tunneling correction (SCT).

(2) The calculated rate constants, activation energies, and branching ratios are discussed. When comparison is available, theoretical results show good agreement with the available experimental data. The three parameter expressions for the title reactions within 200–1,000 K are $k_{1T} = 4.08 \times 10^{-22}$ $T^{3.24}$ $\exp(-631/T)$, $k_{2T} = 6.46 \times 10^{-21}$ $T^{2.90}$ $\exp(-941/T)$, $k_{3T} = 5.53 \times 10^{-22}$ $T^{3.15}$ $\exp(-882/T)$, and $k_{4T} = 3.30 \times 10^{-18}$ $T^{2.10}$ $\exp(-1{,}669/T)$ cm^3 $molecule^{-1}$ s^{-1}, respectively.

(3) Specially, since the reactant $CF_3CF_2CFH_2$ has two stable conformers SC1 with C_s symmetry and SC2 with C_1 symmetry, the total rate constants are obtained by the Boltzmann distribution function. The present calculations suggest that SC2 has predominant contribution to the reaction of $CF_3CF_2CFH_2$ + OH over the whole temperature range, while for $CF_3CF_2CFH_2$ + Cl, SC1 and SC2 are competitive with each other.

(4) Furthermore, the enthalpies of formation of $CF_3CF_2CFH_2$, CF_3CFHCF_2H, CF_3CF_2CFH, CF_3CFCF_2H, and CF_3CFHCF_2 are studied by using isodesmic reactions at BMC-CCSD//BB1K/6-31+G(d, p) and MC-QCISD//BB1K/6-31+G(d, p) levels of theory. And the good agreement is obtained between two high levels of theory, with the largest deviation within 1.0 kcal mol^{-1}.

We hope the theoretical results may be useful for the estimating of the kinetics of the reactions over a wide temperature range where no experimental data are available yet.

Acknowledgments We thank Professor Donald G. Truhlar for providing the POLYRATE 9.3 program. This work was supported by the National Natural Science Foundation of China (20303007, 20333050, and 20073014), the Program for New Century Excellent Talents in University (NCET). The authors are grateful to the referees for their valuable comments on improving the manuscript.

References

1. Garland NL, Medhurst LJ, Nelson HH (1993) J Geophys Res 98:23107. doi:10.1029/93JD02550
2. Atkinson R, Baulch DL, Cox RA, Crowley JN, Hampson RF, Hynes RG, Jenkin ME, Rossi MJ, Troe J, Wallington TJ (2008) Atmos Chem Phys 8:4141
3. Sander SP, Ravishankara AR, Golden DM, Kolb CE, Kurylo MJ, Molina MJ, Moortgat GK, Finlayson-Pitts BJ, Wine PH, Huie RE (2006) JPL Publ 06:2
4. Nelson DD Jr, Zahniser MS, Kolb CE, Magid H (1995) J Phys Chem 99:16301. doi:10.1021/j100044a016
5. Hsu K-J, DeMore WB (1995) J Phys Chem 99:1235. doi:10.1021/j100004a025
6. Zhang Z, Padmaja S, Saini RD, Huie RE, Kurylo MJ (1994) J Phys Chem 98:4312. doi:10.1021/j100067a017
7. Mogelberg TE, Feilberg A, Biessing AMB, Sehested J, Bilde M, Wallington TJ, Nielsen OJ (1995) J Phys Chem 99:17386. doi:10.1021/j100048a013
8. Truhlar DG (1995) In: Heidrich D (ed) The reaction path in chemistry: current approaches and perspectives. Kluwer, Dordrecht, pp 229
9. Truhlar DG, Garrett BC, Klippenstein SJ (1996) J Phys Chem 100:12771. doi:10.1021/jp953748q
10. Hu W-P, Truhlar DG (1996) J Am Chem Soc 118:860. doi:10.1021/ja952464g
11. IUPAC http://www.iupac.org/reports/1999/7110minkin/i.html
12. Frisch MJ, Trucks GW, Schlegel HB, Scuseria GE, Robb MA, Cheeseman JR, Montgomery JA Jr, Vreven T, Kudin KN, Burant JC, Millam JM, Iyengar SS, Tomasi J, Barone V, Mennucci B, Cossi M, Scalmani G, Rega N, Petersson GA, Nakatsuji H, Hada M, Ehara M, Toyota K, Fukuda R, Hasegawa J, Ishida M, Nakajima T, Honda Y, Kitao O, Nakai H, Klene M, Li X, Knox JE, Hratchian HP, Cross JB, Adamo C, Jaramillo J, Gomperts R, Stratmann RE, Yazyev O, Austin AJ, Cammi R, Pomelli C, Ochterski JW, Ayala PY, Morokuma K, Voth GA, Salvador P, Dannenberg JJ, Zakrzewski VG, Dapprich S, Daniels AD, Strain MC, Farkas O, Malick DK, Rabuck AD, Raghavachari K, Foresman JB, Ortiz JV, Cui Q, Baboul AG, Clifford S, Cioslowski J, Stefanov BB, Liu G, Liashenko A, Piskorz P, Komaromi I, Martin RL, Fox DJ, Keith T, Al-Laham MA, Peng CY, Nanayakkara A, Challacombe M, Gill PMW, Johnson B, Chen W, Wong MW, Gonzalez C, Pople JA (2003) Gaussian Inc., Pittsburgh
13. Zhao Y, Lynch BJ, Truhlar DG (2004) J Phys Chem A 108:2715. doi:10.1021/jp049908s
14. Becke AD (1988) Phys Rev A 38:3098. doi:10.1103/PhysRevA.38.3098
15. Becke AD (1996) J Chem Phys 104:1040. doi:10.1063/1.470829

16. Lynch BJ, Zhao Y, Truhlar DG (2005) J Phys Chem A 109:1643. doi:10.1021/jp045847m
17. Chuang YY, Corchado JC, Truhlar DG (1999) J Phys Chem A 103:1140. doi:10.1021/jp9842493
18. Corchado JC, Chuang YY, Fast PL, Hu WP, Liu YP, Lynch GC, Nguyen KA, Jackels CF, Ramos AF, Ellingson BA, Lynch BJ, Melissas VS, Villa J, Rossi I, Coitino EL, Pu J, Albu TV (2005) POLYRATE, version 9.3.1. University of Minnesota, Minneapolis
19. Garrett BC, Truhlar DG (1979) J Chem Phys 70:1593. doi:10.1063/1.437698
20. Garrett BC, Truhlar DG (1979) J Am Chem Soc 101:4534. doi:10.1021/ja00510a019
21. Garrett BC, Truhlar DG, Grev RS, Magnuson AW (1980) J Phys Chem 84:1730 Erratum: (1983) 87: 4554
22. Truhlar DG, Garrett BC (1980) Acc Chem Res 13:440. doi:10.1021/ar50156a002
23. Truhlar DG, Isaacson AD, Garrett BC (1985) Generalized transition state theory. In: Baer M (ed) The theory of chemical reaction dynamics, vol 4. CRC Press, Boca Raton, p 65
24. Truhlar DG, Garrett BC (1984) Annu Rev Phys Chem 35:159. doi:10.1146/annurev.pc.35.100184.001111
25. Lu DH, Truong TN, Melissas VS, Lynch GC, Liu YP, Grarrett BC, Steckler R, Issacson AD, Rai SN, Hancock GC, Lauderdale JG, Joseph T, Truhlar DG (1992) Comput Phys Commun 71:235. doi:10.1016/0010-4655(92)90012-N
26. Liu Y-P, Lynch GC, Truong TN, Lu D-H, Truhlar DG, Garrett BC (1993) J Am Chem Soc 115:2408. doi:10.1021/ja00059a041
27. Garrett BC, Truhlar DG, Wagner AF, Dunning TH (1983) J Chem Phys 78:4400. doi:10.1063/1.445323
28. Garrett BC, Abusalbi N, Kouri DJ, Truhlar DG (1985) J Chem Phys 83:2252. doi:10.1063/1.449318
29. Taghikhani M, Parsafar GA, Sabzyan H (2005) J Phys Chem A 109:8158. doi:10.1021/jp0524173
30. Galano A, Alvarez-ldaboy JR, Ruiz-Santoyo ME, Vivier-Bunge A (2004) Chem Phys Chem 5:1379. doi:10.1002/cphc.200400127
31. Gao H, Wang Y, Liu J, Yang L, Li Z, Sun C (2008) Phys Chem A 112:4176. doi:10.1021/jp077611z
32. Truhlar DG (1991) J Comput Chem 12:266. doi:10.1002/jcc.540120217
33. Chuang YY, Truhlar DG (2000) J Chem Phys 112:1221. doi:10.1063/1.480768
34. Fast PL, Truhlar DG (2000) J Phys Chem A 104:6111. doi:10.1021/jp000408i
35. Lide DR (1999) CRC Handbook of Chemistry and Physics, 80th edn. CRC Press, New York
36. Huber KP, Herzberg G (1979) Molecular spectra and molecular structure, IV: constants of diatomic molecules. Van Nostrand Reinhold, New York
37. Shimanouchi T (1972) Tables of molecular vibrational frequencies consolidated, vol 1. National Bureau of Standards U.S. GPO, Washinton
38. Chase MW, Davies CA, Downey JR, Frurip DJ, MacDonald RA, Syverud AN (1985) JANAF, vol 14 (Suppl 1); American Chemical Society, Washington DC
39. Albu TV, Swaminathan S (2006) J Phys Chem A 110:7663. doi:10.1021/jp0615454
40. Chemistry Webbook NIST, Linstrom PJ, Mallard WG (eds) Available from: http://webbook.Nist.Gov/chemistry
41. Miller WH (ed) (1976) Dynamics of molecular collisions, Part B, vol. 2 of Modern theoretical chemistry, Plenum Press, New York
42. Gilbert RG, Smith SC (1990) Theory of unimolecular and recombination reactions. Blackwell, Oxford
43. Allison TC, Truhlar DG (1998) In: Thompson DL (ed) Modern methods for multidimensional dynamics computations in chemistry. World Scientific, Singapore. p 618
44. Taghikhani M, Parsafar GA (2007) J Phys Chem A 111:8095. doi:10.1021/jp072403s